Journal of Applied Electrochemistry (2005) 35:903–913
DOI 10.1007/s10800-005-4726-5

The electrochemical and electrocatalytic behaviour of glassy metals

H.C. BROOKES[1,*], C.M. CARRUTHERS[1] and T.B. DOYLE[2]
[1]*School of Pure and Applied Chemistry, University of KwaZulu Natal, Durban, 4041, South Africa*
[2]*School of Physics, University of KwaZulu Natal, Durban, 4041, South Africa*
*(*author for correspondence, e-mail: Brookes@nu.ac.za)*

Received 01 February 2002; accepted in revised form 17 March 2005

Key words: electrocatalyst, glassy metals, hydrogen evolution reaction

Abstract

The suitability of a selection of amorphous alloys as electrocatalysts or as inhibitors for hydrogen evolution (HE) was investigated in 1 M KOH at 25 °C. Mild basic conditions were chosen so as to make direct comparison with other data, where available. The alloys studied were the known glassy alloys $Fe_{67}Co_{18}B_{14}Si_1$, $Co_{66}Fe_4Si_{16}B_{12}Mo_2$, $Fe_{40}Ni_{40}B_{20}$ and $Fe_{40}Ni_{40}P_{14}B_6$ and an entirely new glassy alloy $Zr_{73.22}Ti_{19.71}Cu_{1.24}Fe_{5.83}$. The electrochemical techniques of slow sweep anodic and cathodic polarisation were used, in conjunction with the surface analysis techniques of scanning electron microscopy (SEM) and X-ray analysis, to characterise the alloys and new data has been obtained for all alloys. The glassy alloys were tested in their as-polished state, as well as after surface activation, by *ex situ* chemical (acid etching) and *in situ* electrochemical (anodic oxidation in base) pre-treatment. The least corrosion resistant composition, $Fe_{67}Co_{18}B_{14}Si_1$, displayed the highest activity for HE in the as-polished state and only a minor improvement resulted from surface pre-treatment. Corrosion resistance was partly characterised by the degree to which the passive region increased and the passive region current decreased as a function of pre-treatment. The most corrosion resistant alloy, $Zr_{73.22}Ti_{19.71}Cu_{1.24}Fe_{5.83}$, displayed the poorest activity for HE in the as-polished state, but a significant improvement resulted from surface activation by *in situ* anodic oxidation in basic media. Surface activation by acid pre-treatment reduced the corrosion resistance of the $Zr_{73.22}Ti_{19.71}Cu_{1.24}Fe_{5.83}$ alloy and was, therefore, a non-viable and destructive procedure. However, acid pre-treatment was effective in substantially activating the glassy $Co_{66}Fe_4Si_{16}B_{12}Mo_2$ and $Fe_{40}Ni_{40}P_{14}B_6$ alloys towards HE and did not alter the corrosion properties of these compositions. A novel technique for mounting thin alloy specimens has been developed, using an insulating photo-resist coating, resulting in sharply defined electrode edges.

1. Introduction

Metallic alloy glasses represent a class of materials that combine a metallic electronic structure with an amorphous (non-crystalline) molecular structure that lacks the long-range crystalline order present in conventional alloys. They are prepared by rapid solidification of alloy melts, in which cooling rates of 10^6 K/s prevent the nucleation and subsequent growth of a crystalline phase. The rapid quenching process used for the production of the amorphous alloys yields a solid ribbon of about 20–60 μm thickness and 1–25 mm width. Two broad categories of glassy alloys are recognised, namely, metal–metalloid glasses and metal–metal glasses. Metal–metalloid glasses are the most widely studied group, with a metal to metalloid ratio of 4:1 being typical. This consistent glassy forming ratio suggests that a specific type of chemical bonding is present and it is found that alloy compositions that form ''deep eutectics'' in the phase diagram generally display the greatest ease of amorphisation. The metalloid elements are believed to stabilise the amorphous structure by providing an appropriate atomic volume. Certain glassy alloy compositions are of considerable interest, displaying high mechanical strength, corrosion resistance, high magnetic permeability and low coercivity, ductility and enhanced catalytic activity in comparison to crystalline alloys of equivalent composition. Combined with relatively low manufacturing costs, these properties make the alloys attractive for many applications. The practical applications of glassy alloys are limited to those requiring thin layers at low operating temperatures ($\leq$ 600 K) since temperatures approaching the glass transition temperature cause the alloys to rapidly devitrify into their crystalline phase(s) [1–3].

Hydrogen evolution (HE) can occur by an electrocatalytic mechanism at cathode materials via the formation of adsorbed hydrogen intermediates. The reaction proceeds by a two-step pathway involving the adsorption of hydrogen ions onto the electrode material, followed by the formation of molecular hydrogen. Hydrogen desorption can occur by chemical-desorption or by electro-

chemical desorption/ion-atom recombination. The reaction has been widely investigated at a range of different electrode surfaces, in particular at polycrystalline metal and alloy surfaces, and forms a good prototype reaction for investigating the electrocatalytic activity of the relatively newer and less studied group of glassy alloys. HE is of technological importance, since in some processes hydrogen production is desirable (e.g. as the cathode reaction in water electrolysis, in diaphragm and membrane cells for the manufacture of Cl_2, or in hydrogen–oxygen fuel cells) while in other situations it is essential to suppress HE (e.g. as a competing reaction in metal winning, electroplating processes or cathodic syntheses, and to prevent the hydrogen embrittlement of metals). Hydrogen has attracted considerable attention as a possible fuel for the future. The development of efficient and cost effective electrodes for hydrogen generation from water electrolysis and for hydrogen oxidation in power generation from fuel cells is of importance in developing the future hydrogen economy [4]. The commercial success of fuel cells hinges on the development of more efficient, stable and inexpensive electrocatalysts.

The cost of electrolytic hydrogen production is directly related to the overpotential necessary to drive the reaction at a given current density. In general, the overpotentials required are too high to generate hydrogen at a competitive cost and this has slowed the development and commercial utilisation of hydrogen as a fuel. A decrease in overpotential can be obtained by using electrode materials with a high intrinsic activity for HE (for example, expensive single metals such as Pt, Au, Ni, Rh or Ni-based alloys) or by increasing the effective surface area of the electrode. The latter method is perhaps the most successful way of overcoming intrinsically low reaction rates and can be accomplished by surface pre-treatment of the electrodes. Porous electrodes, such as Raney-type Ni catalysts, have greater effective surface areas at which the reaction can occur, resulting in greater apparent current densities.

In general, glassy alloys display a poorer electrocatalytic activity for HE in the as-quenched and as-polished states than their pure major metal components or equivalent crystalline compositions [5–7]. This is attributed to their homogeneous amorphous surface that lacks the defect sites inherent on crystalline surfaces, such as screw or step dislocations, that act as adsorption sites for hydrogen. On the other hand pre-treatment of glassy alloys has been found to activate the alloy surfaces for electrocatalytic reactions, such as HE and oxygen evolution. Chemical pre-treatment of certain glassy alloys with strong oxidising acids increases their effective surface area by selectively dissolving surface oxides and one or more of the alloy components to produce a roughened or porous surface with a greater surface area at which HE can occur [8–11]. An apparent increase in current density results from the greater electrode surface area. In marked contrast, it is reported that the activity of crystalline alloys is not enhanced by chemical pre-treatment but rather that the electrode surface is deactivated or ''poisoned'' [9, 12].

In this study the influence of surface activation of glassy alloys by both chemical and electrochemical pre-treatment, was therefore investigated. Experiments were initially conducted with four metal–metalloid glassy alloys of composition $Fe_{67}Co_{18}B_{14}Si_1$, $Co_{66}Fe_4Si_{16}B_{12}Mo_2$, $Fe_{40}Ni_{40}B_{20}$ and $Fe_{40}Ni_{40}P_{14}B_6$, for which some limited electrochemical data has already been published. The behaviour of the novel four component metal–metal glassy $Zr_{73.22}Ti_{19.71}Cu_{1.24}Fe_{5.83}$ alloy was also investigated, the first such quaternary glassy alloy studied electrochemically, to our knowledge. For all experiments geometrical surface areas were used while being aware that effective electrode areas were probably two to three times greater.

2. Experimental

The four metal–metalloid alloys investigated were obtained commercially and the metal–metal glass was specially prepared. The alloys and their chemical compositions are listed in Table 1. The compositions were measured accurately using a JY 24 Sequential ICP/AES Spectrometer.

The glassy alloys were prepared in ribbon form by melt spinning. The metal–metalloid glasses were ribbons 2–25 mm wide and 0.03–0.06 mm thick while the Zr-based alloy was 10 mm wide and 0.5 mm thick.

A novel technique for mounting the thin glassy alloy specimens was developed so that an evenly polished and reproducible working electrode (WE) surface could be prepared for each experiment. Sections of ribbon (1 cm^2) were secured to a flat Cu-backing (0.9 cm^2) using an epoxy based adhesive (Patex Epoxy Steel, Henkel) that acted as a support for the thin alloy sample and added strength to the final electrode. Without the Cu-backing the alloy-resin contact was weak and the

Table 1. Chemical compositions of the glassy metal alloys (weight%)

Trade name with nominal chemical composition	ICP analysis of chemical composition (weight %)
Allied Chemicals 2605: $Fe_{67}Co_{18}B_{14}Si_1$	$Fe_{68.0}Co_{18.2}Si_{1.5}B_{12.3}$
Vitrovac 0040: $Fe_{40}Ni_{40}B_{20}$	$Fe_{43.2}Ni_{41.4}B_{15.4}$
Vitrovac 6025: $Co_{66}Fe_4Si_{16}B_{12}Mo_2$	$Co_{66.3}Fe_{4.6}Si_{14.8}B_{11.4}Mo_{2.9}$
Allied chemicals 2826: $Fe_{40}Ni_{40}P_{14}B_6$	$Fe_{42.1}Ni_{37.7}P_{14.4}B_{5.8}$
Kirchartov Institute, Moscow	$Zr_{73.22}Ti_{19.71}Cu_{1.24}Fe_{5.83}$

electrode lifted when it was polished and placed in the electrolyte, creating an undefined WE surface. An insulated Cu wire was joined to the back of the alloy sample using silver epoxy cement (Emerson and Cuming, Belgium). The ribbon samples were set in Araldite M resin, and the epoxy mould press fitted into a Teflon holder. The electrodes were mechanically polished to a 0.3 μm Al_2O_3-paste finish. To overcome the problem of poor mechanical adhesion at the electrode–resin interface, the interface was masked with an electrically insulating photo-resist coating (Kodac photo-resist, KPR), leaving only a limited area of the mounted alloy specimen exposed to the electrolyte. The photo-resist emulsion was painted onto the electrode surface, dried and a photographic negative of the required electrode dimension (0.09–0.36 cm^2) placed onto the emulsion. After UV exposure, the unexposed portion of emulsion was removed with the developing agent (KPR developer) to form a sharply defined alloy–photoresist interface with good edge retention.

As an initial electrochemical cleaning procedure, the WE was held at a reducing potential for 10 min in the bulk electrolyte to reduce any air-formed oxide. This regime provided a reproducible electrode surface.

A standard three electrode cell, fitted with a water jacket for temperature control, and containing a spital Pt wire counter electrode and a saturated mercurous sulphate reference electrode (SSE), was used. Experiments were performed in 1 M KOH and all electrolytes were prepared from analytical-grade reagents and ultra-pure deionised water (MILLI-Q water purification system). Prior to experimentation the electrolyte was deoxygenated with high-purity nitrogen (99.998%; < 3 ppm O_2) for 30 min. A nitrogen blanket was maintained over the surface of the electrolyte during each experiment to prevent oxygen from entering the system. The temperature of the electrolyte was controlled at 25 °C ± 0.5 ° C by connecting the cell to a thermostatted water bath.

The potential between the reference electrode and WE was controlled using a BAS CV-27 potentiostat. The current response of the WE was monitored with a digital storage oscilloscope (Nicolet 3091) and transferred to a PC.

The electrocatalytic efficiency of the glassy alloys for HE was determined on the basis of electrochemical data obtained from cathodic polarisation (1 mV/s) in the HE region. Exchange current densities and the Tafel slopes were calculated from Tafel plots. The alloys were tested in their as-quenched state as well as after *ex situ* chemical and *in situ* electrochemical pre-treatment. Chemical pre-treatment involved immersion of the electrodes in pure HF or a mixture of HF and HNO_3 (HF/HNO_3 ratio was 1:4) of different concentrations for different treatment times. Electrochemical pre-treatment involved anodic oxidation at constant currents ranging between 10 and 1000μA cm^{-2} for 2 min using an EG and G 363 Galvanostat/Potentiostat. Geometrical electrode areas were used to calculate initial current densities.

A Hitachi S520 scanning electron microscope (SEM) was used for subsequent qualitative examination of the electrode surface. Quantitative analysis was conducted using a LINK ISIS energy dispersive X-ray spectrometer (EDS). EDS results were reported as weight percentages with a reproducibility of 0.1 wt% obtained at an accelerating voltage of 20 keV. X-ray diffraction was performed using a Philips XRD PW 1730/10 X-ray diffraction machine.

3. Results and discussion

3.1. *As-polished electrodes*

The $Zr_{73.22}Ti_{19.71}Cu_{1.24}Fe_{5.83}$ alloy has not previously been described in the electrochemical literature and is a unique alloy with a substantially greater thickness (~0.5 mm) than the conventional glassy alloys tested (30–60 μm). The composition of the alloy was measured accurately by ICP analysis (Table 1) and an X-ray diffractogram (Figure 1) showed a single broad peak (*d*-spacing of 2.44729) characteristic of a fully amorphous material. Examination of the polished $Zr_{73.22}Ti_{19.71}Cu_{1.24}Fe_{5.83}$ electrode by SEM (Figure 2)

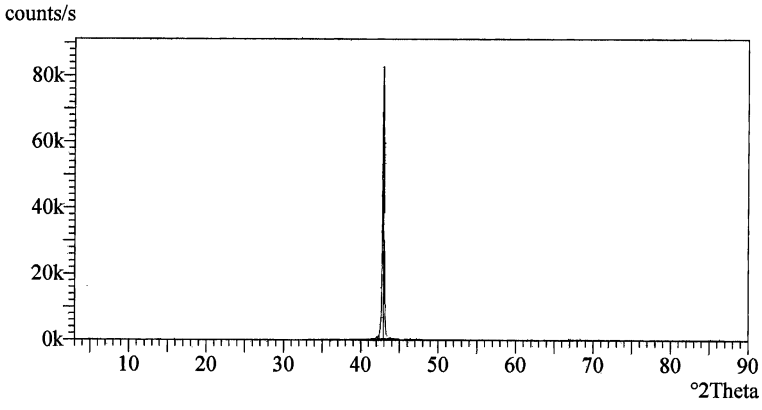

Fig. 1. X-ray diffractogram of the zirconium glassy alloy.

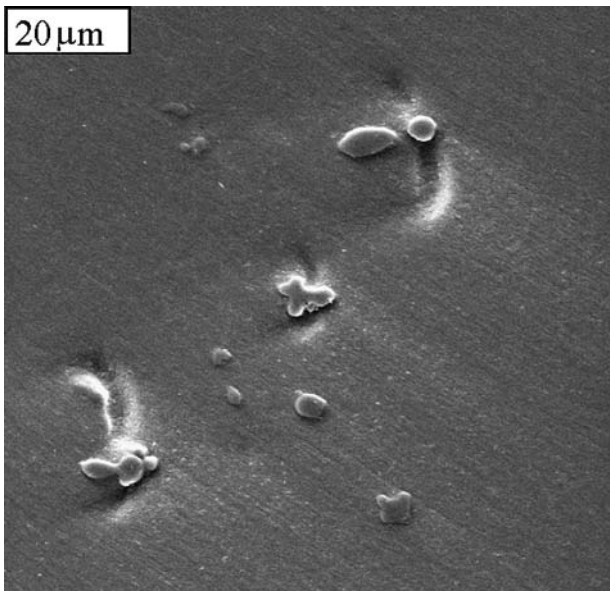

Fig. 2. SEM micrographs of the polished glassy $Zr_{74}Ti_{19}Cu_2Fe_5$ electrode surface, 4000×.

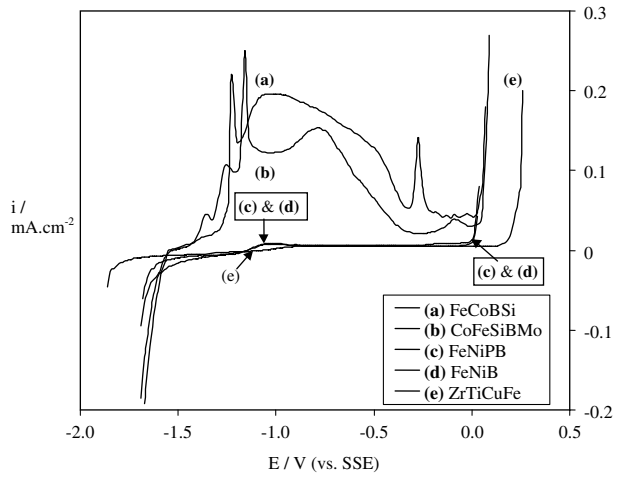

Fig. 3. APC of the glassy alloys in their as-polished state in 1 M KOH at 25 °C (1 mV/s sweep rate).

showed that the surface was not totally homogeneous and supported a few small nodules (3–14 μm diameter) that were firmly embedded and present throughout the entire ribbon thickness. The nodule compositions were 95%Zr and 5%Ti, as indicated by EDS analysis. The occurrence of the nodules suggested that the quench rate of the alloy melt was not sufficiently rapid to prevent partial inhomogeneity of the structure. This highlights the difficulty associated with manufacturing amorphous metal–metal alloys with a homogeneous structure by rapid quenching, particularly ribbons of greater thickness, as here. The exposed surface areas selected for experimentation were those without nodules so as to obtain reproducible electrode surfaces. The thinner metal–metalloid alloy surfaces appeared smooth and homogeneous in comparison to the thicker ribbon when viewed at the same magnification.

3.1.1. *Electrochemical behaviour*

Anodic polarisation curves (APC) of the as-polished glassy alloys provided an indication of their corrosion properties in 1 M KOH at 25 °C (Figure 3). The corrosion potential shifted towards more noble potentials in the order $Co_{66}Fe_4Si_{16}B_{12}Mo_2$ < $Fe_{67}Co_{18}B_{14}Si_1$ < $Fe_{40}Ni_{40}P_{14}B_6$ < $Fe_{40}Ni_{40}B_{20}$ < $Zr_{73.22}Ti_{19.71}Cu_{1.24}Fe_{5.83}$. The corrosion resistance of an alloy is characterised as being greater the more extensive the passive region and the lower the critical current density. On this basis, the $Zr_{73.22}Ti_{19.71}Cu_{1.24}Fe_{5.83}$ alloy displayed the greatest corrosion resistance. No active peak was obtained which indicated that the alloy passivated spontaneously. Transpassivity occurred at potentials greater than 0.16 V, which were substantially higher than the values obtained for the other alloy compositions tested. Clearly the Zr-based glass displays potentially excellent anticorrosive properties in the basic medium.

The glassy $Fe_{67}Co_{18}B_{14}Si_1$ and $Co_{66}Fe_4Si_{16}B_{12}Mo_2$ alloys displayed the poorest passivating abilities in 1 M KOH with high current densities obtained in comparison to the FeNi and ZrTi-based alloys. Both alloys generated several anodic peaks, suggesting that the structure and properties of the anodic film varied with the applied potential. Glassy $Fe_{67}Co_{18}B_{14}Si_1$ produced three anodic peaks at potentials of −1.35, −1.25 and −1.16 V. A broad peak in the potential region of −1.11 to −0.50 V was followed by an active-passive transition at −0.80 V. At potentials greater than −0.80 V a passive region was observed. The current decrease at −0.80 V may be associated with a restructuring of a passive layer or the formation of a new phase or oxide. The shape of the polarisation curve and the magnitude of the current densities obtained at the glassy $Fe_{67}Co_{18}B_{14}Si_1$ electrode was similar to that of glassy $Fe_{60}Co_{20}B_{10}Si_{10}$ (G14) obtained by Crousier et al. [13] in the same medium, suggesting that variation of Si content by a factor of 10 has little effect on these parameters. The cyclic voltammetric response of glassy $Fe_{67}Co_{18}B_{14}Si_1$ showed a close similarity to polycrystalline Fe. Potential cycling between the hydrogen and oxygen evolution regions resulted in progressive disintegration of the alloy by buildup, cracking and flaking of a surface oxide layer.

3.1.2. *Electrocatalytic behaviour*

Typical Tafel plots for HE at the as-polished glassy alloys in 1 M KOH are illustrated in Figure 4. The Tafel regions of the glassy alloys (except for glassy $Fe_{67}Co_{18}B_{14}Si_1$) consisted of two distinct linear Tafel slopes that were divided into regions defined as the low and high overpotential regions. The kinetic data, $i_o(\eta = 0)$ and slopes b, obtained from both regions and their potential limits are listed in Table 2. The electrocatalytic activity of an alloy is characterised as being better the higher the value of i_o and the lower the value of the Tafel slope. As the Tafel slope decreases the current increases,

Table 2. Kinetic data for HE by the glassy alloys in 1 M KOH (25 °C) in the as-polished state and after application of the most activating surface pre-treatments

Alloy	Treatment	High η region			Low η region		
		Tafel range/V	−b /mV	i_o /A cm^{-2}	Tafel range /V	−b /mV	i_o /A cm^{-2}
$Fe_{67}Co_{18}B_{14}Si_1$	As-polished	−1.60 to −1.84	120 ± 7	3.1×10^{-5}			
	1 M HF/1 M HNO_3(1 min)	−1.64 to −1.78	111 ± 3	9.9×10^{-5}			
	500 μA cm^{-2}	−1.66 to −1.78	131 ± 8	7.0×10^{-5}			
$Fe_{60}Co_{20}B_{10}Si_{10}$ Reference [14]	As-polished (25 °C)		95	1.0×10^{-6}			
Reference [13]	As-polished (25 °C)		97	1.4×10^{-6}			
Reference [15]	As-polished (30 °C)		128 ± 7	6.9×10^{-5}			
Reference [13]	500 μA cm^{-2} (25 °C)		135	2.8×10^{-5}			
$Co_{66}Fe_4Si_{16}B_{12}Mo_2$	As-polished	−1.74 to −1.85	103 ± 9	1.5×10^{-5}	−1.61 to −1.74	158 ± 13	8.3×10^{-5}
	1 M HF/1 M HNO_3 (10 min)	−1.68 to −1.82	166 ± 5	2.9×10^{-4}	−1.58 to −1.68	218 ± 17	4.7×10^{-4}
	1000 μA cm^{-2}	−1.72 to −1.84	120 ± 3	7.7×10^{-5}	−1.60 to −1.72	164 ± 4	1.8×10^{-4}
$Fe_{40}Ni_{40}P_{14}B_6$	As-polished	−1.74 to −1.85	72 ± 3	4.6×10^{-7}	−1.63 to −1.74	127 ± 9	6.1×10^{-6}
	1 M HF/1 M HNO_3 (10 min)	−1.70 to −1.78	67 ± 4	1.6×10^{-5}	−1.62 to −1.70	75 ± 2	1.1×10^{-5}
	1000 μA cm^{-2}	−1.71 to −1.84	81 ± 2	1.5×10^{-6}	−1.65 to −1.71	137 ± 18	1.8×10^{-5}
Reference [13]	As-polished (25 °C)		109	1.2×10^{-7}			
Reference [13]	1000 μA cm^{-2} (25 °C)		112	1.6×10^{-6}			
$Fe_{40}Ni_{40}B_{20}$	As-polished	−1.74 to −1.89	117 ± 5	5.6×10^{-6}	−1.65 to −1.74	164 ± 9	1.6×10^{-5}
	1 M HF/1M HNO_3 (10 min)	−1.76 to −1.93	141 ± 1	2.3×10^{-5}	−1.64 to −1.76	188 ± 12	5.3×10^{-5}
	1000 μA cm^{-2}	−1.75 to −1.91	110 ± 6	1.1×10^{-5}	−1.63 to −1.75	187 ± 9	6.4×10^{-5}
Reference [15]	As-polished (30 °C)		174 ± 7	1.3×10^{-4}			
$Zr_{74}Ti_{19}Cu_2Fe_5$	As-polished	−1.84 to −2.10	153 ± 12	4.0×10^{-6}	−1.73 to −1.84	187 ± 11	9.9×10^{-6}
	1 M HF (10 s)	−1.75 to −2.02	172 ± 6	7.9×10^{-5}			
	1000 μA cm^{-2}	−1.88 to −2.12	209 ± 24	3.3×10^{-5}	−1.75 to −1.88	283 ± 25	7.0×10^{-5}

The b and i_o values reported are average values obtained from the Tafel plots of six independent experiments.
Kinetic data for HE by glassy $Fe_{60}Co_{20}B_{10}Si_{10}$, $Fe_{40}Ni_{40}P_{14}B_6$ and $Fe_{40}Ni_{40}B_{20}$ in 1 M KOH as taken from the literature [13, 16, 17] is also reported for comparison.

i.e. the rate at which HE occurs, within the Tafel region, increases. Figure 3 indicates that the relatively poor corrosion resistant $Fe_{67}Co_{18}B_{14}Si_1$ alloy displayed the highest activity for HE in the as-polished state, followed by $Co_{66}Fe_4Si_{16}B_{12}Mo_2$. The glassy $Fe_{40}Ni_{40}B_{20}$ and $Fe_{40}Ni_{40}P_{14}B_6$ alloys were of intermediate activity. The most corrosion resistant glassy alloy, $Zr_{73.22}Ti_{19.71}Cu_{1.24}Fe_{5.83}$, displayed the poorest catalytic activity in the as-polished state and overpotentials significantly lower (more negative) than those of the other alloy compositions were required for HE to occur. This could be attributed to the high corrosion resistance of the alloy and the presence of thin passivating Zr oxide and Ti oxide layers that suppress HE. For all alloys, the high overpotential region displayed a greater activity for HE, i.e. a more rapid increase in current density with increasing overpotential, than the low overpotential region.

In 1 M KOH $Fe_{40}Ni_{40}P_{14}B_6$ Glassy $Fe_{40}Ni_{40}B_{20}$ displayed a higher activity for HE than $Fe_{40}Ni_{40}P_{14}B_6$ in the low overpotential region, while the $Fe_{40}Ni_{40}P_{14}B_6$ alloy displayed a higher activity in the high overpotential region, indicating that the metalloid element P influenced the rate of HE (Figure 4). There is disagreement in the literature as to the influence of metalloid P on the electrocatalytic activity of certain glassy alloys for HE. Lian et al. [10] and Podesta et al. [18] reported that P improved the electrocatalytic activity of the glassy alloys for HE in base while Shervedani and Lasia [19] and Paseka [16] found that amorphous electrodes of lower P content displayed a higher activity for HE in 1 M NaOH (25 °C). Clearly further investigation of the effect of P is required. Only single Tafel values were reported in the literature for HE by the glassy $Fe_{40}Ni_{40}P_{14}B_6$ [13] and $Fe_{40}Ni_{40}B_{20}$ [15] (Table 2). In general the kinetic parameters in the lower overpotential region are less widely reported. Crousier et al. [13] obtained an exchange current of 1.2×10^{-7} Acm^{-2} at glassy $Fe_{40}Ni_{40}P_{14}B_6$ in 1 M KOH (25 °C) that agrees with the value obtained in this study in the high overpotential region while the Tafel slope reported (109 mV) was 37 mV higher than the slope obtained in this study (Table 2). The exchange current density (1.3×10^{-4} Acm^{-2}) and Tafel slope (174 mV) obtained by Kreysa and Hakanson [15] for HE at glassy $Fe_{40}Ni_{40}B_{20}$ did not agree with the values obtained in this study in either overpotential region (Table 2).

3.2. *Acidic pre-treatment of electrodes*

Pre-treatment of alloys with acid was designed to create a reproducible surface for subsequent studies. All acid

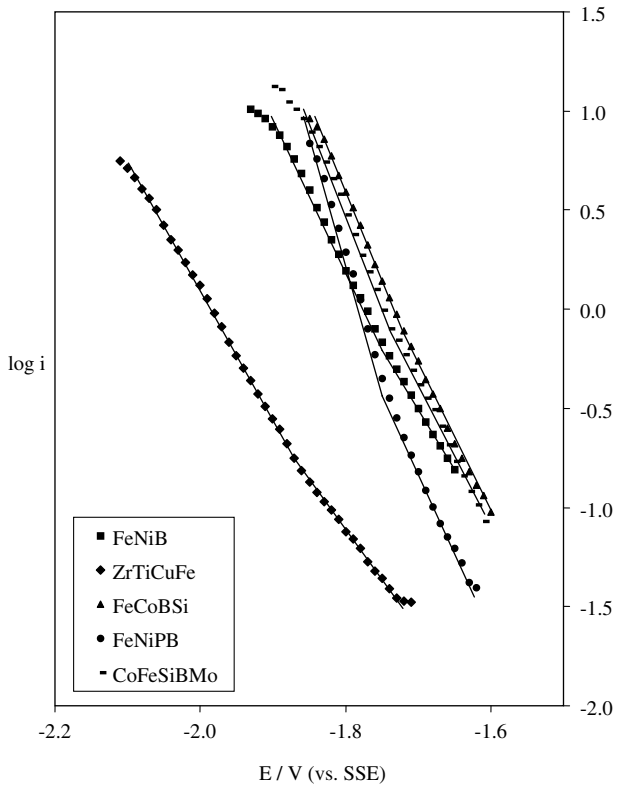

Fig. 4. Typical Tafel plots for HE by the as-polished glassy alloys in 1 M KOH at 25 °C.

pre-treatments improved the activities of the glassy alloys for HE in comparison to their as-polished state. Acid pre-treatment with pure HF was most effective in activating the $Zr_{74}Ti_{19}Cu_2Fe_5$ electrode while HF/HNO_3 mixtures were most effective for the $Co_{66}Fe_4Si_{16}B_{12}Mo_2$, $Fe_{40}Ni_{40}P_{14}B_6$ and $Fe_{40}Ni_{40}B_{20}$ compositions. The Tafel parameters obtained from the most effective acid pre-treatments used on each of the glassy alloys are listed in Table 2.

3.2.1. *Glassy $Fe_{67}Co_{18}B_{14}Si_1$ and $Co_{66}Fe_4Si_{16}B_{12}Mo_2$*

Acid pre-treatment of glassy $Fe_{67}Co_{18}B_{14}Si_1$ was a destructive procedure that produced only minor improvements in the activity of the alloy for HE in comparison to the untreated electrode. All treatments created a visible etch in the alloy surface and treatment with 1 M HF/1 M HNO_3 (5 min) destroyed the alloy sample. Clearly this is undesirable as repeated activation treatments would not produce a stable and long-life catalyst.

Glassy $Co_{66}Fe_4Mo_2Si_{16}B_{12}$ displayed a far greater stability in the acid medium and the electrode showed a substantial improvement in activity for HE after acid pre-treatment. Figure 5 shows a selection of typical Tafel plots produced after *ex situ* acid pre-treatment of glassy $Co_{66}Fe_4Si_{16}B_{12}Mo_2$. Maximum activity was obtained from 1 M HF/1 M HNO_3 (10 min) treatment and the i_o values were 19 and 6 times greater than the values obtained at the as-polished electrode in the high and low overpotential regions respectively. SEM micrographs of portions of the corresponding acid treated electrode surfaces are shown in Figure 6. General surface roughening was evident after acid treatment with 1 M HF/1 M HNO_3 for 1 min (Figure 6a) with the most noticeable etching occurring along the Al_2O_3 polish lines. When the treatment time was extended to 10 min (Figure 6b) a roughened surface with a fine porous structure was produced. It is suggested that acid activation improved the activity of the alloy by increasing its effective surface area and creating a greater number of hydrogen adsorption sites. Current densities were measured according to geometric electrode areas and so a porous surface resulted in greater apparent current densities. This was also supported by the findings of Machida et al. [9].

The corrosion properties of glassy $Co_{66}Fe_4Mo_2Si_{16}B_{12}$ were not altered by acid treatment (1 M HF/1 M HNO_3, 10 min), with all peaks of the anodic polarisation curve occurring at approximately the same potentials as the polished untreated electrode. Greater current densities were obtained in all regions of the acid treated curve and this was attributed to the increased surface area, which resulted in greater apparent current densities. In addition, EDS analysis did not reveal variations in the treated surface compositions in comparison to the as-polished electrode.

After 1 M HF/1 M HNO_3 (10 min) treatment, the i_o values for HE of the glassy $Co_{66}Fe_4Mo_2Si_{16}B_{12}$ alloy

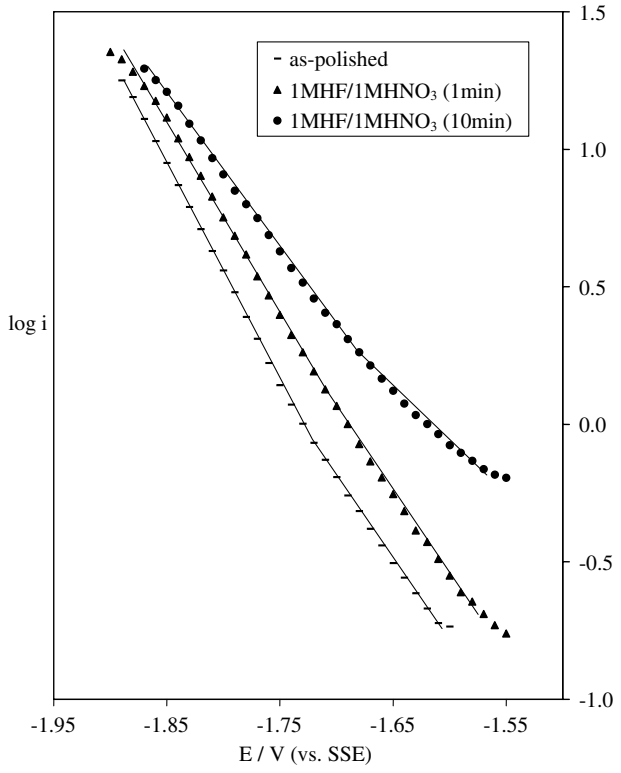

Fig. 5. Typical Tafel plots for HE by glassy $Co_{66}Fe_4Si_{16}B_{12}Mo_2$ in 1 M KOH at 25 °C after surface activation by different *ex situ* acid pre-treatments.

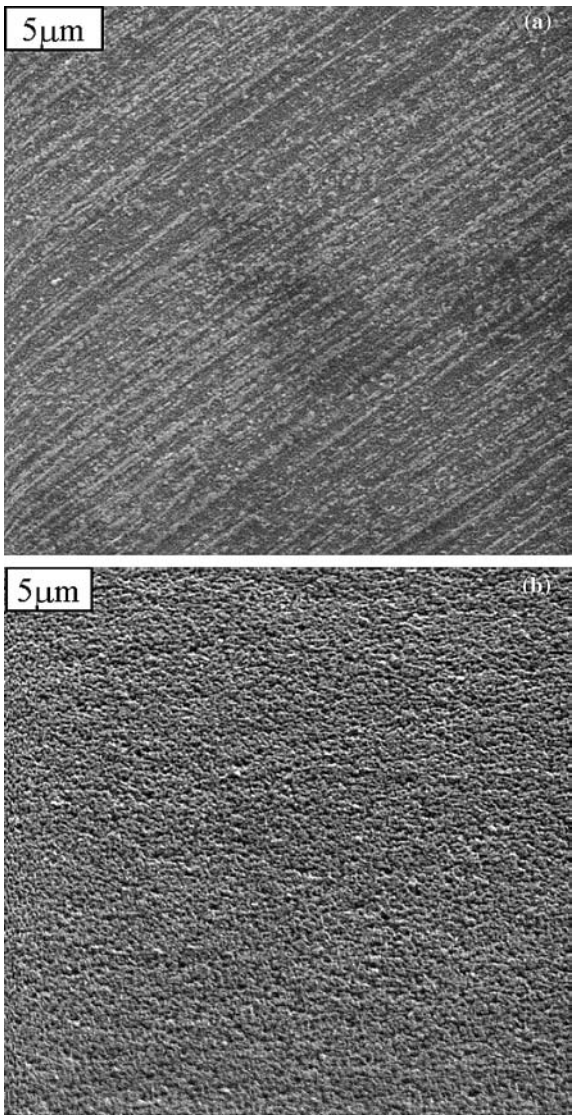

Fig. 6. SEM micrographs of the glassy $Co_{66}Fe_4Si_{16}B_{12}Mo_2$ electrode after acid pre-treatment with 1 M HF/1 M HNO_3 for (a) 1 min and (b) 10 min, 4000×.

were greater than both polycrystalline Fe [20] or Co [14], indicating that the activity of the treated alloy was greater than either alloy components. The i_o values were higher than polycrystalline Pt [14] at 25 °C, however the Tafel slopes were lower, resulting in a lower overall rate of HE by the glassy alloy.

In 1 M KOH $Fe_{67}Co_{18}B_{14}Si_1$ produced i_o values of $3.1 \times 10^{-5}\mu A/cm^2$ (25 °C) and 4.71×10^{-5} $\mu A/cm^2$(30 °C) and b values of −120 mV (25 °C) and −11 6 mV (30 °C) (Table 2). These values are more comparable to the results obtained by Kreysa and Hakansson [15] for the G14 alloy (of similar composition) than those obtained by Crousier et al. [13] and Alemu and Juttner [14]. The surface preparation of the alloy will affect the result obtained. Kreysa and Hakansson and Alemu and Juttner did not describe how they prepared their alloys i.e. whether they were polished the surface or tested the alloy in the as-quenched state. Crousier et al. tested the alloy in the as-quenched state while I polished mine with aluminium oxide powder (to 0.3 μm).

3.2.2. *Glassy $Fe_{40}Ni_{40}P_{14}B_6$ and $Fe_{40}Ni_{40}B_{20}$*

Acid pre-treatment with 1 M HF/1 M HNO_3 (10 min) produced a much greater increase in the activity of the $Fe_{40}Ni_{40}P_{14}B_6$ alloy for HE than identical treatment of the $Fe_{40}Ni_{40}B_{20}$ composition. The i_o value of glassy $Fe_{40}Ni_{40}P_{14}B_6$ was 35 times greater than the as-polished electrode while the $Fe_{40}Ni_{40}B_{20}$ alloy was only 4.2 times greater in the high overpotential region. The $Fe_{40}Ni_{40}P_{14}B_6$ electrode was P-enriched in the as-quenched state with a surface P-content of 16.80wt% measured by EDS. After 1 M HF/1 M HNO_3 (10 min) treatment, the surface P-content measured was 10.55 wt%, indicating that P was selectively leached from the alloy surface. SEM analysis of the acid treated $Fe_{40}Ni_{40}P_{14}B_6$ electrode showed that it was highly roughened and numerous small craters produced a porous structure that enhanced the electrode surface area in comparison to the as-polished surface. The roughened surface probably provided a greater surface area at which HE could occur and increased the rate of the reaction. A much lower degree of surface roughening resulted from equivalent acid treatment of the P-free glassy alloy composition.

The APC for the acid treated glassy $Fe_{40}Ni_{40}P_{14}B_6$ and $Fe_{40}Ni_{40}B_{20}$ alloys had similar shapes to those found using untreated surfaces, indicating that the corrosion properties of the alloys were unchanged. The current densities measured at the $Fe_{40}Ni_{40}P_{14}B_6$ electrode were greater than the $Fe_{40}Ni_{40}B_{20}$ electrode in all regions of the APC after identical treatments. This supported our SEM findings that indicated that the increased surface area of the porous $Fe_{40}Ni_{40}P_{14}B_6$ electrode was responsible for the greater activity of the alloy.

Aqueous HF treatment was less effective than the HF/HNO_3 mixture in improving the activity of the glassy FeNi-based alloys for HE. The glassy $Fe_{40}Ni_{40}P_{14}B_6$ and $Fe_{40}Ni_{40}B_6$ compositions were susceptible to hydrogen absorption as evidenced by blister formation and rupturing on the alloy surfaces after HF treatment. Both glassy $Fe_{40}Ni_{40}P_{14}B_6$ and $Fe_{40}Ni_{40}B_{20}$ are reported to be susceptible to hydrogen absorption and embrittlement [10, 20–22].

The glassy $Fe_{40}Ni_{40}P_{14}B_6$ and $Fe_{40}Ni_{40}B_{20}$ alloys were less active for HE in their as-polished state than their polycrystalline Fe [20] and Ni [23] components at 25 °C. After acid pre-treatment (1 M HF/1 M HNO_3, 10 min), the i_o values of glassy $Fe_{40}Ni_{40}P_{14}B_6$ were similar to those reported for Fe and Ni. The Tafel slopes of the glassy alloy were lower in both overpotential regions than Fe and Ni, indicating that the current density increased more rapidly at the alloy surface to produce a greater overall activity for HE. It is noteworthy that we find that the i_o values of the alloy were of the same magnitude as polycrystalline Pt [14] while the Tafel slopes of the alloy were lower in value, indicating that

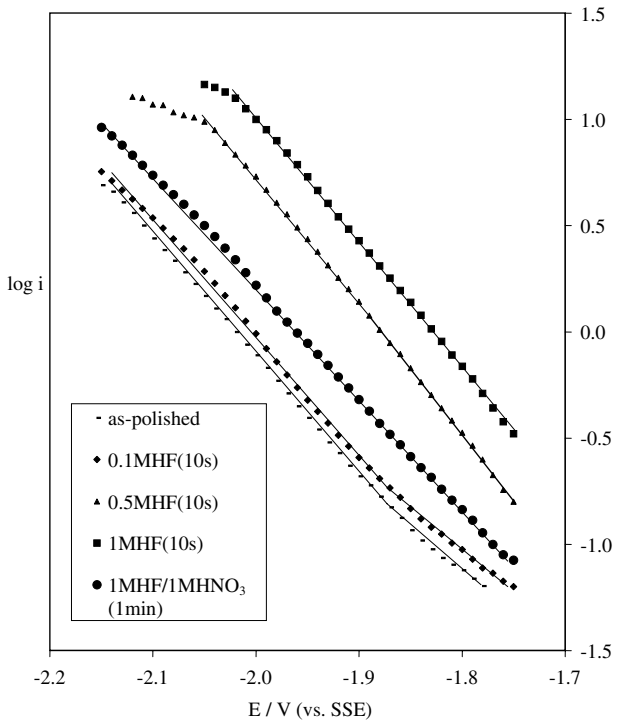

Fig. 7. Typical Tafel plots for HE by glassy $Zr_{74}Ti_{19}Cu_2Fe_5$ in 1 M KOH at 25 °C after surface activation by different *ex situ* acid pre-treatments.

the activity of the glassy alloy was also greater after acid pre-treatment than polycrystalline Pt.

3.2.3. *Glassy $Zr_{73.22}Ti_{19.71}Cu_{1.24}Fe_{5.83}$*

A substantial increase in the electroacatalytic activity of the novel glassy $Zr_{73.22}Ti_{19.71}Cu_{1.24}Fe_{5.83}$ alloy for HE resulted from acid pre-treatment. Typical Tafel plots obtained after acid pre-treatment are shown in Figure 7. Pure HF (10 s) was most effective in activating this alloy and the i_o value obtained was 19.6 times greater than the value obtained at the smooth, polished electrode in the high overpotential region. The order in which acid treatment increased the activity of the alloy was 1 M HF/HNO_3 (10 s) < 0.1 M HF (10 s) < 1 M HF/HNO_3 (1 min) < 0.5 M HF (10 s) < 1 M HF (10 s). This contrasted with the glassy $Fe_{40}Ni_{40}B_{20}$, $Fe_{40}Ni_{40}P_{14}B_6$ and $Co_{66}Fe_4Si_{16}B_{12}Mo_2$ compositions which showed the greatest improvements in activity after acid pre-treatment with the HF/HNO_3 mixture and reasons for this reversal are unknown. Only single Tafel slopes were obtained after the more severe acid treatments of glassy $Zr_{73.22}Ti_{19.71}Cu_{1.24}Fe_{5.83}$ with 0.5 M HF (10 s), 1.0 M HF (10 s) and 1 M HF/1 M HNO_3 (1 min). The slopes were similar in value and an average slope of 176 mV was obtained. This value was 20 mV higher than the Tafel slope obtained for the polished alloy in the high overpotential region.

A SEM micrograph of a portion of the $Zr_{73.22}Ti_{19.71}Cu_{1.24}Fe_{5.83}$ electrode (Figure 8a) showed that the most activating acid treatment (1 M HF, 10 s) created a porous surface. The increased current densities can, in part, be attributed to the porous alloy surface that resulted in greater apparent current densities. EDS analyses indicated that acid treatment selectively leached the Zr component of the alloy from the electrode surface and resulted in a corresponding enrichment of the Ti, Cu and Fe components. The surface Zr content decreased by 7.86 wt% after 1 M HF treatment (10 s) in comparison to the as-polished electrode. Chemical activation has been proposed to occur by dissolution of the surface oxide layer(s) that inhibit HE, followed by selective dissolution of the Zr component from the alloy. HF-pre-treatment has been found to be particularly effective in activating the surface of Zr-based glassy alloys for HE in comparison to their as-quenched state [9, 23]. Spriano et al. [23] reported that HF treatment of glassy $Zr_{64}Ni_{36}$ and $Zr_{48}Ni_{27}Al_{25}$ resulted in selective dissolution of the Zr component to create a Ni-enriched surface. XRD indicated that particles of crystalline Ni

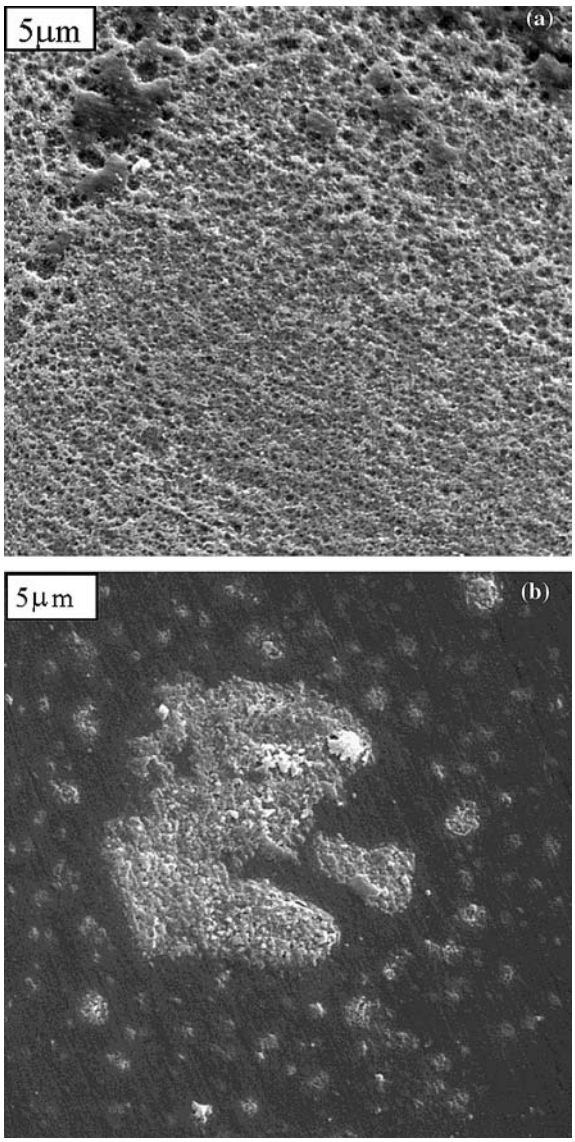

Fig. 8. SEM micrographs of the glassy $Zr_{74}Ti_{19}Cu_2Fe_5$ electrode after acid pre-treatment with (a) 1 M HF treatment (10 s) and (b) anodic oxidation at 1000 μA cm^{-2} (2 min), mag. 4000×.

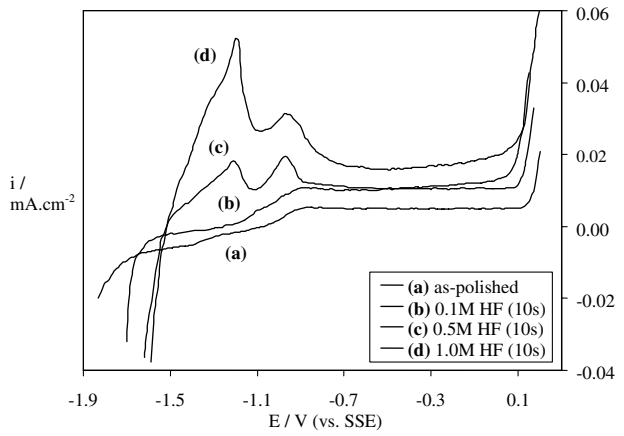

Fig. 9. APC of the glassy $Zr_{74}Ti_{19}Cu_2Fe_5$ electrode in 1 M KOH at 25 °C after surface activation by different *ex situ* acid pre-treatments (1 mV/s sweep rate).

formed on the alloy surface and that these contributed to the high activity of these alloys.

APC show that acid treatment reduced the corrosion resistance of the $Zr_{73.22}Ti_{19.71}Cu_{1.24}Fe_{5.83}$ electrodes in comparison to the as-polished state (Figure 9). HF pre-treatment resulted in a voltammogram with an active region consisting of two anodic peaks, at potentials of −1.20 and −0.97 V, indicating that primary and secondary active-passive transitions occurred with increasing potential. The HF/HNO_3 treated surfaces showed no sign of passivation and a progressive increase in current density resulted for potentials more positive than the corrosion potential. Hence, the beneficial effect of acid pre-treatment in activating the alloy surface for HE was countered by a reduction in the general corrosion resistance of the alloy.

In the as-polished state the $Zr_{73.22}Ti_{19.71}Cu_{1.24}Fe_{5.83}$ electrode displayed a lower activity for HE, in both the high and low overpotential regions, than both polycrystalline Ni [23] and Pt [14] at 25 °C, i.e. lower exchange currents and higher Tafel slope values were obtained for the $Zr_{73.22}Ti_{19.71}Cu_{1.24}Fe_{5.83}$ alloy. The i_o value of $Zr_{74}Ti_{19}Cu_2Fe_5$ after 1 M HF (10 s) treatment was greater than polycrystalline Ni [23] and Pt [14] while the Tafel slope of the glassy alloy was 52 mV higher than Pt, indicating that overall the rate of HE at the alloy surface was slower than at the Pt surface.

3.3. *Anodic pre-treatment of electrodes*

In view of the dramatic effect on HE shown by prior ex *situ* (acidic) oxidation of the glassy alloy surfaces, the influence of *in situ* (anodic) oxidation in the basic medium was also investigated for comparison. The kinetic parameters obtained from the most activating anodic pre-treatments of each of the glassy alloys are listed in Table 2.

Anodic pre-treatment was more effective in activating the glassy $Zr_{73.22}Ti_{19.71}Cu_{1.24}Fe_{5.83}$ alloy for HE than the other glassy alloys tested. Results showed that the activity of the alloy increased progressively as the magnitude of the oxidation current was increased. A maximum activity resulted from anodic oxidation at 1000 μA cm^{-2} (2 min) and the i_o values obtained were 8.2 and 7.0 times greater in the high and low overpotential regions respectively than those of the as-polished electrode. This increase was lower than the increase obtained after 1 M HF pre-treatment (10 s), however, the APC of the anodically treated $Zr_{73.22}Ti_{19.71}Cu_{1.24}Fe_{5.83}$ surfaces (Figure 10) indicate that this treatment did not have a detrimental effect on the corrosion properties of the alloy. In this regard, anodic pre-treatment would produce a more durable and long-life electrocatalyst, in comparison to acid activation, and is the preferred technique for activating the glassy $Zr_{73.22}Ti_{19.71}Cu_{1.24}Fe_{5.83}$ electrode for the HE.

SEM analysis of the anodically treated $Zr_{73.22}Ti_{19.71}Cu_{1.24}Fe_{5.83}$ electrode surface showed that the treatment produced a surface deposit, possibly an oxide, consisting of discrete patches that became more extensive as the oxidation current was increased (Figure 8b). EDS analysis is not sufficiently sensitive to measure the composition of these thin surface deposits as distinct from the underlying alloy composition. The surface deposit increased the electrode surface area and appeared to provide new and catalytically active surface sites for HE. Importantly, a change in the nature of the hydrogen adsorption sites after anodic pre-treatment was indicated by a change in the Tafel slope values and also a change in the shape of the APC in comparison to the as-polished electrode. The question of finding the composition of extremely thin passivating or activation layers on crystalline metal or vitreous substrates is a perennial one. No sufficiently sensitive technique is available to give unambiguous answers to the prime question regarding the nature of such layers when analysed *in vacuo* as compared to their nature *in situ* i.e in aqueous solution in our case. It seems quite probable that these thin metal oxyhydroxide layers will change in

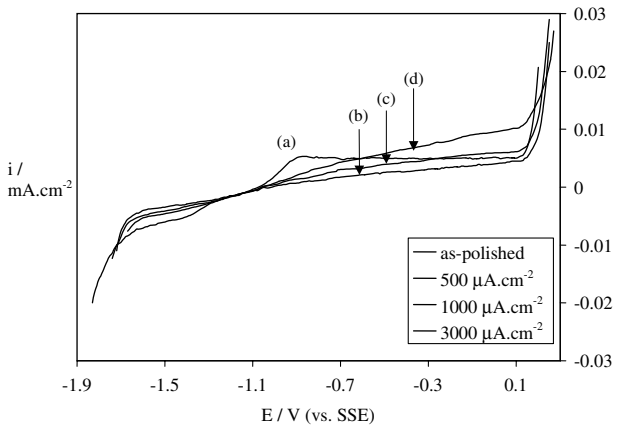

Fig. 10. APC of the glassy $Zr_{74}Ti_{19}Cu_2Fe_5$ electrode in 1 M KOH at 25 ° C after different *in situ* anodic pre-treatments (1 mV/s sweep rate).

nature from in solution to *in vacuo*. Hence we have not pursued this question.

Anodic treatment of the glassy $Fe_{40}Ni_{40}P_{14}B_6$ and $Fe_{40}Ni_{40}B_{20}$ resulted in only a slight improvement in the activity of these compositions in comparison to their as-polished states. The activities of both alloys improved as the magnitude of the oxidation current was increased to a maximum activity obtained after an anodic treatment of 1000 μA cm^{-2} (2 min). SEM and EDS analysis revealed no visible or compositional changes in the alloy surface after anodic treatment indicating that this method of activation was far less effective than acid pre-treatment. The i_o values obtained at the $Fe_{40}Ni_{40}P_{14}B_6$ electrode in the high overpotential region compared closely to the value obtained by Crousier et al. [13]. However, Crousier et al. only reported a single Tafel slope that was 31 mV higher than the value obtained in this study.

Glassy $Fe_{67}Co_{18}B_{14}Si_1$ showed a maximum activity for HE after anodic oxidation at 500 μA cm^{-2} (2 min). Further increase in the oxidation current resulted in a decrease in the activity of the alloy. This trend was also reported to occur at the glassy $Fe_{60}Co_{20}B_{10}Si_{10}$ alloy of similar composition [13] and the exchange current and Tafel slope obtained at 500 μA cm^{-2} (2 min) compared closely with the values obtained for glassy $Fe_{67}Co_{18}B_{14}Si_1$ (Table 2). SEM analysis of the alloy surface showed a very fine and evenly distributed surface deposit that increased in thickness as the oxidation current was increased. Again, EDS analysis did not have sufficient sensitivity to measure the composition of this surface layer. In similar findings, Hout et al. [20] reported that anodic pre-treatment of glassy $Fe_{60}Co_{20}B_{10}Si_{10}$ at constant current density in 30 wt% KOH resulted in the formation of a black surface deposit of Fe_3O_4, proposed to form by a dissolution-precipitation mechanism involving Fe(II) species. Subsequent cathodic reduction prior to the onset of HE created a porous layer of Fe-rich particles that created catalytically active surface sites. The particle layer increased the electrode surface area and resulted in an increase in the current density and hence an improved electrocatalytic activity. A similar effect is suggested to have occurred at the $Fe_{67}Co_{18}B_{14}Si_1$ electrode surface after anodic oxidation.

4. Conclusions

A new glassy metal, $Zr_{73.22}Ti_{19.71}Cu_{1.24}Fe_{5.83}$, has been characterised and its behaviour compared with that of known glasses under similar conditions. The corrosion behaviour and HE capability of all alloys are compared. For all glassy alloy compositions tested, chemical pre-treatment was more effective than anodic pre-treatment in activating the alloy surfaces for HE. The least corrosion resistant glassy alloy, $Fe_{67}Co_{18}B_{14}Si_1$, displayed the highest activity for HE in the as-polished but did not show a significant increase in activity after acid pre-treatment prior to polarisation in 1 M KOH. In comparison, acid pre-treatment did not alter the corrosion properties of the glassy $Co_{66}Fe_4Si_{16}B_{12}Mo_2$ and $Fe_{40}Ni_{40}P_{14}B_6$ alloys and 1 M HF/1 M HNO_3 (10 min) treatment was found to be the most effective method of activating both these alloy compositions. The HE properties of these glasses are reported. SEM analysis showed that the electrode surfaces of both glasses were highly roughened by acid pre-treatment in comparison to the smooth as-polished electrodes, the roughened $Fe_{40}Ni_{40}P_{14}B_6$surface resulting from selective dissolution of the P-component from the alloy. In comparison the P-free glassy alloy, $Fe_{40}Ni_{40}B_{20}$, did not show a similar increase in activity for HE after the same acid pre-treatment. The activity of the highly corrosion resistant $Zr_{73.22}Ti_{19.71}Cu_{1.24}Fe_{5.83}$ alloy was low in the as-polished state but was significantly improved by acidic pre-treatment in 1 M HF (10 s). Acid pre-treatment produced a highly roughened electrode surface by selective dissolution of the Zr component from the alloy and also resulted in a large decrease in corrosion resistance of the alloy. Anodic pre-treatment of glassy $Zr_{73.22}Ti_{19.71}Cu_{1.24}Fe_{5.83}$ (3000 μA cm^{-2} for 2 min) increased the activity of the alloy for HE and did not alter the corrosion properties of the alloy.

A novel method of precisely mounting and defining these thin vitreous metals as electrodes has been developed.

Acknowledgements

We acknowledge financial support from the University of Natal Research Fund and the Foundation for Research and Development (R.S.A.).

References

1. M.D. Archer, C.C. Corke and B.H Harji, *Electrochim. Acta* **32** (1987) 13.
2. J.J. Gilman, *Science* **208** (1980) 856.
3. A.L. Greer, *Science* **267** (1995) 1947.
4. J. O'M. Bockris and A.K. Reddy, 'Modern Electrochemistry', Vol. 2 (Plenum Press, New York, 1977) 1328, 1351 pp.
5. R. Schlogel, 'Rapidly Quenched Metals' (Elsevier Publishers, Lausanne, 2003) 1723 pp.
6. W.E. Brower, M.S. Matyjaszczyk, T.L. Pettit and G.V. Smith, *Nature* **301** (1983) 497.
7. D.L. Cocke, *J. Metals* (1986) 70.
8. K. Machida, M. Enyo, T. Toyoshima, K. Miyahara, K. Kai and K Suzuki, *Bull. Chem. Soc. Jpn.* **56** (1983) 3393.
9. K. Machida, M. Enyo, K. Kai and K Suzuki, *J. Less-Common Metals* **100** (1984) 377.
10. K. Lian, D.W. Kirk and S.J Thorpe, *Electrochim. Acta* **36** (1991) 537.
11. M. Enyo, T. Yamazaki, K. Kai and K Suzuki, *Electrochim. Acta* **28** (1983) 1573.
12. N. Kumagai, Y. Samata, A. Kawashima, K. Asami and K Hashimoto, *J. Appl. Electrochem.* **17** (1987) 347.

13. J. Crousier, J.P. Crousier and F Bellucci, *Electrochim. Acta* **38** (1993) 821.
14. H. Alemu and K Juttner, *Electrochim. Acta* **33** (1988) 1101.
15. G. Kreysa and B Hakansson, *J. Electroanal. Chem.* **201** (1986) 61.
16. I Paseka, *Electrochim. Acta* **40** (1995) 1633.
17. J.Y. Huot and L Brossard, *Int. J. Hydrogen Energy* **12** (1987) 599.
18. J.J. Podesta, R.C.V. Piatti, A.J. Arvia, P. Ekdunge, K. Juttner and G Kreysa, *Int. J. Hydrogen Energy* **17** (1992) 9.
19. R.K. Shervedani and A Lasia, *J. Electrochem. Soc.* **144** (1997) 511.
20. J.Y. Huot, M. Trudeau, L. Brossard and R Schulz, *J. Electrochem. Soc.* **136** (1989) 2224.
21. L. Vracar and B.E Conway, *J. Electroanal. Chem.* **227** (1990) 253.
22. R.M. Latanision and H Opperhause, *Met. Trans.* **5** (1974) 483.
23. S. Spriano, M. Baricco, C. Antonione, E. Angelini, F. Rosalbino and P Spinelli, Electrochim. *Acta* **39** (1994) 1781.